AIAA–2000–0097
Correlation Between Geometric Similarity of Ice Shapes and the Resulting Aerodynamic Performance Degradation—A Preliminary Investigation Using WIND

William B. Wright
Dynacs Engineering Company, Inc.
Brook Park, OH
and
James Chung
Institute for Computational Mechanics in Propulsion
Cleveland, OH

38th Aerospace Sciences Meeting & Exhibit
January 10–13, 2000 / Reno, NV

NASA/CR—1999-209417 AIAA–2000–0097

Correlation Between Geometric Similarity of Ice Shapes and the Resulting Aerodynamic Performance Degradation—A Preliminary Investigation Using WIND

William B. Wright
Dynacs Engineering Company, Inc., Brook Park, Ohio

James Chung
Institute for Computational Mechanics in Propulsion, Cleveland, Ohio

December 1999

The NASA STI Program Office . . . in Profile

Since its founding, NASA has been dedicated to the advancement of aeronautics and space science. The NASA Scientific and Technical Information (STI) Program Office plays a key part in helping NASA maintain this important role.

The NASA STI Program Office is operated by Langley Research Center, the Lead Center for NASA's scientific and technical information. The NASA STI Program Office provides access to the NASA STI Database, the largest collection of aeronautical and space science STI in the world. The Program Office is also NASA's institutional mechanism for disseminating the results of its research and development activities. These results are published by NASA in the NASA STI Report Series, which includes the following report types:

- TECHNICAL PUBLICATION. Reports of completed research or a major significant phase of research that present the results of NASA programs and include extensive data or theoretical analysis. Includes compilations of significant scientific and technical data and information deemed to be of continuing reference value. NASA's counterpart of peer-reviewed formal professional papers but has less stringent limitations on manuscript length and extent of graphic presentations.

- TECHNICAL MEMORANDUM. Scientific and technical findings that are preliminary or of specialized interest, e.g., quick release reports, working papers, and bibliographies that contain minimal annotation. Does not contain extensive analysis.

- CONTRACTOR REPORT. Scientific and technical findings by NASA-sponsored contractors and grantees.

- CONFERENCE PUBLICATION. Collected papers from scientific and technical conferences, symposia, seminars, or other meetings sponsored or cosponsored by NASA.

- SPECIAL PUBLICATION. Scientific, technical, or historical information from NASA programs, projects, and missions, often concerned with subjects having substantial public interest.

- TECHNICAL TRANSLATION. English-language translations of foreign scientific and technical material pertinent to NASA's mission.

Specialized services that complement the STI Program Office's diverse offerings include creating custom thesauri, building customized data bases, organizing and publishing research results . . . even providing videos.

For more information about the NASA STI Program Office, see the following:

- Access the NASA STI Program Home Page at ***http://www.sti.nasa.gov***

- E-mail your question via the Internet to help@sti.nasa.gov

- Fax your question to the NASA Access Help Desk at (301) 621-0134

- Telephone the NASA Access Help Desk at (301) 621-0390

- Write to:
  NASA Access Help Desk
  NASA Center for AeroSpace Information
  7121 Standard Drive
  Hanover, MD 21076

NASA/CR—1999-209417 AIAA–2000–0097

Correlation Between Geometric Similarity of Ice Shapes and the Resulting Aerodynamic Performance Degradation—A Preliminary Investigation Using WIND

William B. Wright
Dynacs Engineering Company, Inc., Brook Park, Ohio

James Chung
Institute for Computational Mechanics in Propulsion, Cleveland, Ohio

Prepared for the
38th Aerospace Sciences Meeting and Exhibit
sponsored by the American Institute of Aeronautics and Astronautics
Reno, Nevada, January 10–13, 2000

Prepared under Contract NAS3–98008

National Aeronautics and
Space Administration

Glenn Research Center

December 1999

Acknowledgments

The authors would like to thank the NASA Glenn Icing Branch and the Aviation Operations Safety Project Office for their continued support of this research, both financially and for their help with this report. Special recognition goes to Gene Addy for providing the experimental data included in this report.

Available from

NASA Center for Aerospace Information
7121 Standard Drive
Hanover, MD 21076
Price Code: A03

National Technical Information Service
5285 Port Royal Road
Springfield, VA 22100
Price Code: A03

AIAA-2000-0097

Correlation Between Geometric Similarity of Ice Shapes and the Resulting Aerodynamic Performance Degradation - A Preliminary Investigation Using WIND

William B. Wright *
Dynacs Engineering Co., Inc.
Brook Park, OH

James Chung *
Institute for Computational Mechanics in Propulsion
Cleveland, OH

I. Abstract

Aerodynamic performance calculations were performed using WIND[1] on ten experimental ice shapes and the corresponding ten ice shapes predicted by LEWICE 2.0[2]. The resulting data for lift coefficient and drag coefficient are presented. The difference in aerodynamic results between the experimental ice shapes and the LEWICE ice shapes were compared to the quantitative difference in ice shape geometry presented in an earlier report[3]. Correlations were generated to determine the geometric features which have the most effect on performance degradation. Results show that maximum lift and stall angle can be correlated to the upper horn angle and the leading edge minimum thickness. Drag coefficient can be correlated to the upper horn angle and the frequency-weighted average of the Fourier coefficients. Pitching moment correlated with the upper horn angle and to a much lesser extent to the upper and lower horn thicknesses.

II. Nomenclature

a_k	Fourier transform coefficient (dimensionless)
C_d	drag coefficient (dimensionless)
$C_{l,max}$	maximum lift coefficient (dimensionless)
C_m	pitching moment coefficient (dimensionless)
E_2	frequency-weighted average of the Fourier coefficients (dimensionless)
f_k	spacial frequency (cycles/(s/c))
f_s	sampling frequency (cycles/(s/c))
m_e	a geometric measurement made on an experimental ice shape (dimensions depend upon which measurement)
m_L	a geometric measurement made on a LEWICE generated ice shape (dimensions depend upon which measurement)
m_{ref}	reference geometric measurement used for nondimensionalization (dimensions depend upon which measurement)
n	number of points on geometry
OCF	Overall Comparison Factor (dimensionless)
R	regression coefficient (dimensionless)
$R_{measurement}$	regression coefficient on a given geometric measurement (dimensionless)
R_{effect}	regression coefficient for a multiple variable regression equation for a given aerodynamic effect (dimensionless)
t_l	lower surface maximum thickness (inches); lower horn thickness
t_{le}	leading edge minimum thickness (inches)
t_u	upper surface maximum thickness (inches); upper horn thickness
w_f	weighting factor (dimensionless)
α_{stall}	stall angle (degrees)
δ	normalized segment length

* Senior Member, AIAA

(dimensionless)

θ_u angle at upper maximum thickness (degrees); upper horn angle

III. Introduction

In the past, ice accretions acquired by different means (flight tests, tunnels, tankers, or computer codes) have mostly been compared to each other by comparing the ice shape geometry for the various ice accretions[4-8]. Historically, this geometric comparison has also been qualitative rather than quantitative. This makes it difficult to compare the similarity of different geometries with a resulting difference in aeroperformance. Recently, two methods have been proposed by which different ice shape geometries could be compared in a quantitative and objective manner[9-10]. For many applications however, it is the degradation of aerodynamic performance due to the ice shape which is of primary concern. It is usually taken for granted that similar ice shapes will exhibit similar degradation.

Authors in the past have investigated the similarity of aerodynamic performance with changes in the ice shape[11-13], but the investigations used qualitative comparisons of the ice accretions and did not include the variety of shapes used in the present investigation. The approach used in this report was similar to the approach used by Gray[14], except more ice geometry terms were considered and lift and pitching moment were analyzed as well. More recently, Papadakis et. al.[15] investigated aerodynamic effects on a spoiler plate attached to the leading edge to simulate an ice accretion while Kim and Bragg[16] used a simplified horn shape. Both investigations looked at the aerodynamic effect for different sizes and locations of the protrusion. However, the correlation between the aerodynamic effects on these simplified geometries and actual ice shapes has not been established.

In this paper, the quantitative differences in aerodynamic performance for 20 ice shapes were compared to the geometric comparison in order to develop a correlation between the aerodynamic performance and the ice shape geometry. This correlation can then be used to reduce the number of geometric measurements which need to be taken and to provide a more meaningful geometric comparison method. Since experimental aerodynamic data is both time consuming and expensive to obtain, the initial investigation will use calculated flow results generated by the WIND[1] Naviér-Stokes code. This investigation will be useful to provide trends so that fewer test points will be necessary to validate the resulting correlation.

Two ice shapes were chosen for each meteorological condition; one ice shape generated by the NASA Glenn Icing Research Tunnel (IRT) in a previously reported test[17] and the corresponding ice shape predicted by LEWICE 2.0[2]. The ice shapes which were chosen for this investigation reflect a wide range of comparison from the geometric comparison technique. Based on the quantitative parameters used by the first author in a previous report[9], the variation of the LEWICE generated ice shapes was between 2.6% to 20% from the experimental values. Results presented consist of the aerodynamic degradation of the ice shapes in terms of the lift and drag coefficients as well as the pitching moment calculated by WIND up to the stall condition. Post-stall behavior was not investigated at this time. Trends for the variation of these coefficients with increasing variability of the ice shape measurements will be noted. These trends can be compared to the experimental studies performed by Kim and Bragg[16] and by Papadakis, et. al.[15].

The report was divided into four sections. The first sections will provide a brief description of LEWICE and the WIND Naviér-Stokes code used for the aerodynamic predictions. The next section will describe the experimental data used for this comparison and the last section will show the results of the comparison.

IV. LEWICE 2.0

The computer code LEWICE embodies an analytical ice accretion model that evaluates the thermodynamics of the freezing process that occurs when supercooled droplets impinge on a body. The atmospheric parameters of temperature, pressure, and velocity, and the meteorological parameters of liquid water content (LWC), droplet diameter, and relative humidity are specified and used to determine the shape of the ice accretion. The surface of the clean (un-iced) geometry is defined by segments joining a set of discrete body coordinates. The code consists

of four major modules. They are 1) the flow field calculation, 2) the particle trajectory and impingement calculation, 3) the thermodynamic and ice growth calculation, and 4) the modification of the current geometry by addition of the ice growth.

LEWICE applies a time-stepping procedure to "grow" the ice accretion. Initially, the flow field and droplet impingement characteristics are determined for the clean geometry. The ice growth rate on each segment defining the surface is then determined by applying the thermodynamic model. When a time increment is specified, this growth rate can be interpreted as an ice thickness and the body coordinates are adjusted to account for the accreted ice. This procedure is repeated, beginning with the calculation of the flow field about the iced geometry, then continued until the desired icing time has been reached.

LEWICE 2.0 is different from its predecessors not through wholesale changes in the physical models but rather through an extensive effort to adjust, test and document the code to ensure: that the code runs correctly for all of the cases shown; that the quality of output is maintained across platforms and compilers; that the effects of time step and spacing have been minimized and demonstrated; that the code inputs and outputs are consistent and easy to understand; that the structure and documentation within the code makes it readily modifiable to those outside the standard LEWICE development team; and that the code has been validated in a quantified manner against the largest possible amount of experimental data.

V. WIND

WIND is a general purpose Reynolds averaged Naviér-Stokes flow analysis code supported by the NPARC Alliance[1]. In WIND, the Naviér-Stokes equations are written in delta form using a node-centered finite-volume approach. Specification of the discretization of the equations of motion on the right-hand side is modular and flexible. Complex geometries can generally be handled with ease by the multi-block capability and modular boundary conditions. Inviscid, laminar, and turbulent flows can be simulated for 2-D (or axi-symmetric) and 3-D geometries. The code also has Runge-Kutta and Global Newton schemes for time accurate computations. For the simulation of turbulent flows, WIND offers algebraic, one-equation, and two-equation turbulence models. In this study, the Spalart-Allmaras[18] one-equation turbulence model was used. In a previous study, it was found to give the best results for iced airfoils[19]. At the far field boundary, a non-reflecting type boundary condition was applied. GRIDGEN[20], a publicly available multi-block grid generator, was used to create the grids for this study.

VI. Description of Test Data

The test data chosen for this study was part of the NASA Modern Airfoil Program[17]. An airfoil was chosen from this data set so that the results would be more directly applicable to the needs of industry. The airfoil chosen from this data set was the GLC305 airfoil which is shown in Figure 1. This airfoil was chosen as it will be the focus of an upcoming test in the Low Turbulence Pressure Tunnel (LTPT) at NASA Langley. This test will collect aerodynamic performance data on the clean airfoil and several ice shapes, including ice shapes used in this report. Hence, it will be possible in the future to compare the calculated results from WIND with this data set.

The GLC305 airfoil used in the IRT test had a seventy-two inch span and a chord of thirty-six inches. Pressure tap and wake survey data were also taken on this model in the IRT, so this data could also be used for comparison. A total of seventy-two runs were made in the icing tunnel in two test entries during 1995 and 1996.

From this data, ten ice shapes were selected for comparison. Due to time constraints, not every ice shape from Ref. 9 can be analyzed. The ten shapes were chosen to represent a wide variety of shapes from rime ice to glaze ice, and to represent a wide range of geometric comparison with the ice shapes calculated by LEWICE. The ice shapes are shown in Figures 2-11. Based on the quantitative parameters presented in the LEWICE Validation Report[9], the ten figures were ordered so that the most geometrically similar comparisons are shown in Figure 2, while the least geometrically similar are shown in Figure 11. The other figures were similarly ordered from the more similar shapes to the least similar. The factors used for this ranking were the geometric factors used in the previous report[9].

VII. Results

VII. 1 WIND Results

The first step in acquiring results was to join each of the tracings of the experimental ice shapes to the airfoil. Normally, only the ice shape is traced and digitized in the experiment which results in an open curve in front of the airfoil. Due to small errors in tracing, this shape may not intersect the airfoil geometry. A tangent line was drawn from the ice shape to attach the experimental ice shapes to the airfoil. After that step, a two block grid was generated for each case. The two blocks consisted of a dense inner block grid near the airfoil surface and a sparser grid for the far field. This was done so that the grid lines could be better controlled around the complex ice shapes used in this study. The outer block resolution was 125x21 and started at a distance of 0.5 chord from the airfoil.

The inner grid had 71 points normal to the surface and ended at 0.6 chord from the airfoil, resulting in an overlap grid boundary. This grid overlap was generated to meet the requirements of the NPARC code so that later code comparisons could be made.Smoothing of the ice shapes was avoided unless absolutely necessary in order to obtain a quality grid. Grid resolution in the chordwise direction varied from 260 points to 450 points depending upon the complexity of the ice shape. Due to time constraints, a detailed grid sensitivity study was not performed. Instead, the researchers relied upon previous experience with grid generation of ice shapes[19]. The flow conditions used as inputs into WIND were based upon the LTPT test matrix for the cases which are scheduled to be run for that test. For the other ice shapes, the flow conditions simulated the conditions used to generate the ice shape in the IRT. All of the flow conditions were very similar and have been listed in Table 1. Due to time constraints, Reynolds number effects could not be included in the study.

Calculations were performed every 2° angle of attack, starting at 0° on each ice shape. Near stall, runs were made every angle of attack. A total of 183 runs were made with WIND for this study. Post processing included calculating lift coefficient, drag coefficient and pitching moment for each case. Figures 12-21 show the lift curves for the twenty ice shapes. In each of these plots the resulting lift calculated by WIND for the LEWICE generated ice shape was compared to the results for the experimental ice shape. Figures 12-14 show very close agreement for lift between the ice shapes which was in good agreement with both the qualitative and quantitative assessment of the geometric differences. The lift predictions were further apart in other figures which also tracks the widening difference in geometry between the experimental ice shape and the shape predicted by LEWICE. An exception can be seen in Figure 18 and the corresponding ice shapes in Figure 8. The difference in geometry was fairly small, but there was a large difference in the lift degradation between the two shapes. This was attributed to the sharp corner on the upper surface of the experimental ice shape which caused flow separation while the LEWICE generated ice shape was a smooth curve. This may indicate that additional geometric parameters such as horn curvature may need to be included in the analysis.

Figures 22-31 show the drag results calculated by WIND for the same ice shapes. Again, the drag results for the LEWICE generated ice shapes were compared to the values generated on the experimental ice shapes. The drag coefficients for the clean airfoil were shown for reference. Figures 22-24 show close agreement between the results on the experimental ice shape and those generated on the LEWICE ice shape which corresponds to the geometric agreement. As seen with the lift data, as the difference in geometry becomes greater, the difference in drag between the two ice shapes increases as well. An exception can be seen in the drag comparison of Figure 31 and the corresponding ice shape in Figure 11. Here the drag coefficients were reasonably close to each other even though the ice shapes were very dissimilar. It was also notable that some cases exhibited a much higher increase in drag due to ice when compared to the remaining cases. This effect can be correlated with the geometric parameters as described in the next section.

The moment coefficients for these cases are shown in Figures 32-41. In these cases, it was more difficult to assess qualitative trends in the curves with differences in the geometries. Runs 916 and 941, shown in Figures 39-40, show similar performance results although the ice shape geometries were not similar in shape. Comparatively, the performance results were more dissimilar for Runs 937, 204 and 907 as shown in Figures 32, 33 and 35 although the geometries were much closer. Once again, the next

section will examine the correlation between geometric differences and the aerodynamic differences for these cases.

VII. 2 Statistical Results

This section will analyze the resulting lift, drag and moment results and compare them to the quantitative differences in geometry as reported in the LEWICE validation report[9] and to the parameters calculated by Ruff[10] in his report. This comparison will determine which geometric parameters have the strongest correlation with the aerodynamic results. A strong correlation will mean that those geometric parameters should be given more weight when determining an overall geometric parameter and can also be used to reduce the number of geometric measurements which need to be calculated on a given ice shape.

The geometric measurements reported in the LEWICE validation report were: lower icing limit; upper icing limit; lower maximum thickness (lower horn length); leading edge thickness; upper maximum thickness (upper horn length); lower surface ice area; upper surface ice area; total ice area; lower horn angle, upper horn angle, and the difference between the upper and lower horn angles. These measurements are shown in Figures 42 and 43. Additional geometric measurements of maximum width, impingement width, stagnation thickness and maximum thickness were added from Ruff's report and are also represented in these figures. The two Fourier transform parameters described in that report were also used. The first Fourier parameter was the maximum coefficient and was shown by Ruff to be an indicator of the size of the ice shape. The second parameter was the frequency-weighted normalized difference in Fourier coefficients over the entire spectrum. This parameter indicates not only the size of the ice shape but also the relative roughness or irregularity of the ice shape. The maximum Fourier coefficient is given by the equation

$$|a_k|_{max} = max\left|\frac{1}{n}\sum_{j=0}^{n-1}\delta(j)\exp\left(-2\pi i\frac{jk}{n}\right)\right| \qquad (1)$$

where $\delta(j)$ is an array containing the normalized length of each segment and n is the number of points. The second Fourier parameter is given by the equation

$$E_2 = \sum_{f_k=0}^{100}\frac{1}{f_k}\frac{|a_{f_k,iced} - a_{f_k,clean}|}{|a_{f_k,iced} + a_{f_k,clean}|} \qquad (2)$$

where f_k is the spatial frequency which is given by

$$f_k = \frac{k}{n-1}\frac{f_s}{2} \qquad (3)$$

and f_s is the sampling frequency.

For both the geometric and Fourier terms, the comparison performed in this report used the actual measurements and values. The percentage differences and normalized differences were not used. For each parameter, a scatter plot such as the one shown in Figure 44 was generated. This figure plots the maximum lift coefficient predicted by WIND as a function of the upper horn angle for all twenty ice shapes. A least-squares curve fit was also generated to show the level of agreement. In this example, the correlation was quite strong, with an R^2 value of 0.74. Similar curve fits were generated for the other geometric measurements.

A stepwise regression was then performed to determine which of the factors were considered statistically significant correlations. In a stepwise regression, the correlations were systematically compared by considering only the variable which correlates the best and then measures the relative importance of the other variables independently of that factor. The process was continued until none of the remaining variables was considered to correlate with the results using a 95% confidence interval. The regression can also be performed backwards, whereby the variables which correlate the least were eliminated one by one until only those which correlate within the 95% confidence level remain. Both forward and backwards stepwise regressions were used in this analysis. The results shown in this paper represent forward stepwise regression unless otherwise noted. The commercial program STATVIEW was used to perform the calculations. Using the results of that analysis, a multi-variable regression curve-fit can be generated which can be used as a correlation between the geometric measurements and the performance results.

The results of this analysis show that for the maximum lift coefficient and stall angle predicted by WIND, the two geometric factors which showed a statistically significant correlation were the upper horn angle and the leading edge ice thickness. The fre-

quency-weighted Fourier parameter was also found to be somewhat significant, although much less so than the geometric factors. The correlations for the primary variables are shown in Figures 44-47 along with the regression curve fits. The correlation for lift coefficient versus horn angle and leading edge ice thickness was stronger than similar curves using the stall angle since the stall angle was resolved only to the nearest degree. The multiple regression equations determined by the forward stepwise regression are shown below.

$$C_{l,max} = -0.077 + 0.84\left(\frac{\theta_u}{180}\right) + 0.181 t_{le} \quad (4)$$

with an $R^2 = 0.822$

$$\alpha_{stall} = 2.925 + 5.44\left(\frac{\theta_u}{180}\right) + 1.525 t_{le} \quad (5)$$

with an $R^2 = 0.797$. When the frequency-weighted Fourier parameter was added to the lift correlation, the equation became

$$C_{l,max} = -0.102 + 0.693\left(\frac{\theta_u}{180}\right) + 0.186 t_{le} - 0.509 E2 \quad (6)$$

Equations 2 and 3 were then used to calculate an expected $C_{l,max}$ and α_{stall}. These calculated values are plotted against the values predicted by WIND in Figures 48 and 49. All of these curves have positive correlations. For upper horn angle, this means that a higher horn angle produced larger lift degradation and a lower stall angle than a lower horn angle. This is illustrated in Figure 50. A higher horn angle in this sense means that the tip of the horn is relatively higher (largest y-value). Based upon the definition of horn angle, which corresponds to the definition used in the LEWICE validation report[9], a horn angle with a higher peak value actually results in a smaller reported horn angle. For the leading edge ice thickness, it means that a smaller thickness yielded a larger lift degradation and a smaller stall angle as shown in Figure 51. Since the majority of ice shapes studied in this example were large glaze ice shapes, this can be interpreted as meaning that a lower freezing fraction at the leading edge produced a more well-defined ice horn and hence reduced the maximum lift coefficient. This was interpreted to mean that glaze ice shapes will exhibit more performance degradation than a rime or mixed shape which had the same upper surface angle.

Based upon this observation, it might be expected that the upper and lower horn thicknesses should also show a correlation. This was not found to be the case however. The correlation for upper horn thickness was especially poor, as shown in Figure 52. This can be attributed to the fact that the runback water from the leading edge was distributed on the both the upper and lower surfaces and contributes to horn width as well as thickness. Other geometric factors which measured the 'glazeness' of the ice shape could be derived to investigate this conclusion. The Fourier parameter, E2, becomes larger with increasing size or complexity of the ice shape. A negative coefficient in Equation 3 means that as the ice shape becomes larger or more complex, the maximum lift decreases. In this way, the overall shape factor shows the effect of increasing ice size which could not be seen from the horn thickness measurements.

For the drag and pitching moment results, the correlations were performed at each angle of attack. For example, a correlation was made between the drag coefficient at 0° angle of attack for each ice shape and the various ice shape parameters. Initially, this analysis was performed using only the geometric parameters as the Fourier terms require a specialized program to analyze the shapes. A measurement method which could be used in an icing tunnel or in flight would have to be based on the geometric parameters which would not require digitalization except to enhance the accuracy of the calculation.

The regression analysis procedure described earlier was performed to determine the most significant features. The results of this analysis show that the upper horn angle and the upper horn thickness were the most significant geometric factors for the drag coefficient. For each angle of attack in the range 0° to 6° both parameters were considered statistically significant within the 95% confidence interval. For angles of attack of 7° and 8°, only the upper horn angle was within this interval. Above this angle, no correlation was found since the flow around many of the ice shapes had stalled. This result may be due to limitations of the WIND code and the turbulence model in predicting stall behavior. An example of the regression curve fits is shown in Figure 53. This plot shows a fairly low regression coefficient but it still indicates that ice shapes with higher horn angles (lower θ_u values) will generally exhibit a higher drag. There was an additional trend in this analysis which

showed that at 0° angle of attack, the upper horn thickness correlates better, while the horn angle correlates better at higher angles. This is shown in Table 2. This table also shows some extremely low regression coefficients for upper horn thickness which calls into question the result. However, for secondary factors, the stepwise regression method looks at the effect of the second factor after the effect of the primary factor has been removed. Once this was done, then the correlations were much higher. The regression equations for drag using the geometric factors are given below.

$$C_{d,\alpha=0} = 0.053 - 0.052\left(\frac{\theta_u}{180}\right) + 0.012 t_u \quad (7)$$

$R^2 = 0.574$

$$C_{d,\alpha=2} = 0.067 - 0.063\left(\frac{\theta_u}{180}\right) + 0.009 t_u \quad (8)$$

$R^2 = 0.474$

$$C_{d,\alpha=4} = 0.1 - 0.094\left(\frac{\theta_u}{180}\right) + 0.011 t_u \quad (9)$$

$R^2 = 0.509$

$$C_{d,\alpha=5} = 0.128 - 0.118\left(\frac{\theta_u}{180}\right) + 0.012 t_u \quad (10)$$

$R^2 = 0.529$

$$C_{d,\alpha=6} = 0.156 - 0.143\left(\frac{\theta_u}{180}\right) + 0.014 t_u \quad (11)$$

$R^2 = 0.54$

$$C_{d,\alpha=7} = 0.181 - 0.138\left(\frac{\theta_u}{180}\right) \quad (12)$$

$R^2 = 0.459$

$$C_{d,\alpha=8} = 0.222 - 0.169\left(\frac{\theta_u}{180}\right) \quad (13)$$

$R^2 = 0.468$

The correlation of drag with the upper horn angle and upper horn thickness was first reported by Gray[14] in 1958. However, in both that report and in this study, there was significant scatter in the data. This indicates that other factors are important which were not covered by the geometric measurements. The Fourier transform coefficients were then added to the analysis to determine their importance. This analysis shows that the frequency-weighted average of the Fourier coefficients was the most significant factor for drag at lower angles of attack and equally significant to the upper horn angle at higher angles, as shown in Table 3. The stepwise regression was then repeated including this factor. The results of that analysis showed that the upper horn thickness was no longer a significant factor except at α=0° as shown in the equations below. This occurs because horn thickness was shown by Ruff to be a portion of the Fourier coefficients, therefore the small correlation due to that measurement was included and enhanced by using the Fourier coefficients. The modified regression equations for drag are given below.

$$C_{d,\alpha=0} = 0.039 - 0.038\left(\frac{\theta_u}{180}\right) + 0.034E2 + 0.01 t_u \quad (14)$$

$R^2 = 0.664$

$$C_{d,\alpha=2} = 0.038 - 0.025\left(\frac{\theta_u}{180}\right) + 0.062E2 \quad (15)$$

$R^2 = 0.530$

$$C_{d,\alpha=4} = 0.063 - 0.046\left(\frac{\theta_u}{180}\right) + 0.082E2 \quad (16)$$

$R^2 = 0.590$

$$C_{d,\alpha=5} = 0.084 - 0.063\left(\frac{\theta_u}{180}\right) + 0.098E2 \quad (17)$$

$R^2 = 0.625$

$$C_{d,\alpha=6} = 0.106 - 0.081\left(\frac{\theta_u}{180}\right) + 0.113E2 \quad (18)$$

$R^2 = 0.635$

$$C_{d,\alpha=7} = 0.139 - 0.105\left(\frac{\theta_u}{180}\right) + 0.126E2 \quad (19)$$

$R^2 = 0.639$

$$C_{d,\alpha=8} = 0.167 - 0.124\left(\frac{\theta_u}{180}\right) + 0.139E2 \quad (20)$$

$$R^2 = 0.642$$

Note that although the correlation coefficients have increased, they remain much lower than the coefficients obtained during the lift analysis. This indicates that there are still other factors which remain to be determined. This can be illustrated in Figure 54, which shows the drag coefficient predicted by the correlation relative to the drag coefficient predicted by WIND.

The correlations were positive correlations so from the equations, a higher upper horn angle (smaller θ_u) produced a higher drag coefficient as well as a lower lift coefficient as shown earlier. For the upper horn thickness, a larger value increased the drag coefficient. These trends are illustrated in Figure 55. The Fourier term increases with increasing ice size and complexity, so the regression equation shows that larger ice shapes in general produce more drag and that more complex (rougher) ice shapes will have higher drag coefficients than smoother ice shapes.

A similar regression analysis was then applied to the pitching moment coefficients. Once again, the analysis was generated at each angle of attack to determine the most important features. The results of this analysis showed that at 0° angle of attack, the most significant geometric terms were the upper horn angle and the lower horn thickness while at angles of attack from 4° to 7°, the significant terms were the upper horn angle and the upper horn thickness. At an angle of attack of 2°, only the upper horn angle correlated. Above 7°, no correlations were found due to the onset of stall for many ice shapes as described earlier. Even at 7°, the correlation coefficient was 0.319, which was marginal. Once again, the most influential measurement was the upper horn angle as illustrated by the regression plot in Figure 56. The results in this figure show significant scatter at the higher horn angles (lower θ_u values) but there was a general trend where less degradation from the clean results was seen when the upper horn angle was below the horizontal ($\theta_u > 180°$).

Regression equations for pitching moment can be generated for these factors as was done for lift and drag. The results of that effort are shown below. An interesting trend was seen in the effect of horn thickness. At 0° angle of attack, the pitching moment was increased as the lower horn thickness increased. Similarly, the effect of increasing upper horn thickness was to decrease pitching moment at the higher angles of attack. Since a positive moment in this case was a pitch down moment, this was understandable as the increase in length caused an increase in flow around the horn. The same trend was evidenced in the upper horn angle. As θ_u increases, this caused the airfoil to pitch down more. These trends can be seen in Figure 57.

$$C_{m,\alpha=0} = -0.031 + 0.054\left(\frac{\theta_u}{180}\right) + 0.009t_l \quad (21)$$

$$R^2 = 0.735$$

$$C_{m,\alpha=2} = -0.053 + 0.076\left(\frac{\theta_u}{180}\right) \quad (22)$$

$$R^2 = 0.611$$

$$C_{m,\alpha=4} = -0.073 + 0.105\left(\frac{\theta_u}{180}\right) - 0.012t_u \quad (23)$$

$$R^2 = 0.733$$

$$C_{m,\alpha=5} = -0.066 + 0.093\left(\frac{\theta_u}{180}\right) - 0.012t_u \quad (24)$$

$$R^2 = 0.742$$

$$C_{m,\alpha=6} = -0.057 + 0.079\left(\frac{\theta_u}{180}\right) - 0.011t_u \quad (25)$$

$$R^2 = 0.684$$

$$C_{m,\alpha=7} = -0.018 + 0.03\left(\frac{\theta_u}{180}\right) - 0.006t_u \quad (26)$$

$$R^2 = 0.319$$

The correlation equations above can be used to predict the pitching moment as was seen for the lift and drag results. This can be seen in Figure 58 which shows the predicted pitching moment at an angle of attack of 6°. As was the case for the drag results, there was significant scatter in this plot which again indicates that additional factors are important which are not captured by the current geometric measures. This can also be seen in Table 4, which shows the

individual regression coefficients for each factor. As was the case with the drag results, the horn thicknesses are clearly secondary factors to the upper horn angle.

VII. 3 Implications for LEWICE Comparisons

Once the geometric measurements important to aerodynamic performance have been identified, those measurements can be used in the evaluation criteria which compares LEWICE results to experimental ice shapes. A revised overall comparison factor has been derived based upon the aerodynamic results which emphasizes the relative importance of each factor. In every case, it was shown that the upper horn angle was a significant term. Other factors such as the leading edge minimum thickness (for $C_{l,max}$ and α_{stall}) and the frequency-weighted average of the Fourier coefficients (for drag) were very significant as well. The upper and lower horn thicknesses can be added as secondary factors. The comparison factor which has been derived uses the regression coefficients for each of the parameters as the weighting factors. The numbers were then normalized to produce a percentage difference. The equation below shows the result of this process.

$$w_f = \left(\frac{R^2_{measurement}}{\sum R^2_{measurement}} \right) \left(\frac{R^2_{effect}}{\sum R^2_{effect}} \right) \quad (27)$$

where $R^2_{measurement}$ was the average regression fit for the individual measurement and R^2_{effect} was the average regression fit of the effect. In this way, the measurements which correlate the best will have higher weights.

For example, the $R^2_{measurement}$ for the leading edge minimum thickness was the average of the R^2 obtained by the regressions for $C_{l,max}$ and α_{stall}, or 0.7125 and the $R^2_{measurement}$ for the upper horn angle for the same two regressions was 0.7085. The average $R^2_{measurement}$ for the Fourier term E2 was 0.1225 since the R2 with respect to lift was 0.245 and it did not correlate with α_{stall}. The sum of these terms was 1.5435. The average correlation for the lift effects ($C_{l,max}$ and α_{stall}) was 0.8095. Doing these calculations for the drag and pitching moment terms shows that the sum of the R^2_{effect} terms was 2.0677 which becomes the normalization factor in Equation 24. The overall contribution of the leading edge minimum thickness was then

$$w_f = \left(\frac{0.7125}{1.5435} \right) \left(\frac{0.8095}{2.0677} \right) = 0.181 \quad (28)$$

Table 5 shows the weighting factors and relative weights for each measurement. This table shows that the highest weighting factor was found for the upper horn angle. This was expected as it was found to be a significant term for every aerodynamic effect investigated. The table also shows the small effect of either horn thickness as the correlation coefficients were low. These weighting factors were then applied to the comparison of the ten LEWICE ice shapes to each of the ten experimental ice shapes using the equation below.

$$OCF = \sum_i w_{f_i} \left(\frac{|m_e - m_L|}{m_{ref}} \right)_i \quad (29)$$

In this equation, OCF is a revised Overall Comparison Factor, $w_{f,i}$ are the weighting factors from Table 5 and m_e and m_L are the measured values for each parameter for the experimental ice shape and the LEWICE ice shape respectively. The reference measurement m_{ref} was the factor used to nondimensionalize the measurements as defined in the previous report[9]. The frequency-weighted average of the Fourier coefficients was a dimensionless term, therefore $m_{ref} = 1$. For the horn angle, the values were converted to radians to make them dimensionless. Table 6 shows the comparison factors for each case along with the change in lift, stall angle, drag and pitching moment between the experiment and the LEWICE prediction. In this table, the absolute differences were shown. For drag and pitching moment, the value listed was the average of the absolute differences at each angle of attack. Although the agreement was not perfect, there was evidence of the general trends presented earlier. In particular, ice shapes which were found to be close geometrically were also close in performance. However, a large difference in ice shape did not always result in larger differences in aerodynamic performance.

VIII. Conclusions

Aerodynamic predictions were made using the WIND code on ten experimental ice shapes and on the corresponding ten LEWICE ice shapes at angles of attack from 0° up to stall. Performance measurements of lift coefficient, drag coefficient and pitching moment were presented. A regression analysis was performed to express the performance variables as linear combinations of geometric measurements of the ice shapes, including parameters calculated using Fourier Transform methods. A statistical analysis was performed to determine the most important geometric measurements for maximum lift coefficient, stall angle, drag coefficient and pitching moment.

The measurements which had the highest correlation for maximum lift coefficient and stall angle were the upper horn angle and the leading edge minimum thickness, the latter being a measure of the glazeness of the ice. The frequency-weighted average of the Fourier coefficients (E2) was found to be a secondary factor for the maximum lift coefficient. The most important measurements for drag coefficient were the frequency-weighted average of the Fourier coefficients and the upper horn angle. When only the geometric parameters are used, the upper horn thickness became a secondary factor. For pitching moment, the primary measurement was the upper horn angle with a very slight secondary effect due to the upper and lower horn thicknesses.

Correlation equations were generated based upon a multiple variable regression analysis. These equations were then used to determine weighting factors for a revised comparison factor which could be used to compare two separate ice shapes. This comparison factor compares favorably with both a qualitative assessment of the geometric differences and with the aerodynamic performance results. Future work in this area includes validation of the trends and of the WIND code using experimental data and the extension of this analysis to other types of airfoils and an investigation of Reynolds Number effects.

IX. References

1 Bush, R. H., Power, G. D., and Towne, C. E., "WIND: The Production Flow Solver of the NPARC Alliance," AIAA 98-0935, Jan. 1998.

2 Wright, W. B., "Users Manual for the NASA Lewis Ice Accretion Code LEWICE 2.0," NASA CR209409, Sept. 1999.

3 Wright, W. B., "A Summary of Validation Results for LEWICE 2.0," AIAA 99-0249, Jan. 1999.

4 Wright, W. B., Gent, R. W. and Guffond, D., "DRA/NASA/ONERA Collaboration on Icing Research Part II – Prediction of Airfoil Ice Accretion," NASA CR202349, May 1997.

5 Gent, R. W., "TRAJICE2 – A Combined Water Droplet and Ice Accretion Prediction Codes for Airfoils," RAE TR 90054, 1990.

6 Hedde, T. and Guffond, D., "Improvement of the ONERA 3-D Icing Code, Comparison with 3D Experimental Shapes," AIAA 93-0169, Jan. 1993.

7 Brahimi, M. T., Tran, P., and Paraschivoiu, I., "Numerical Simulation and Thermodynamic Analysis of Ice Accretion on Aircraft Wings," Centre de Développement Technologique de l'École Polytechnique de Montréal, C. D. T. Project C159, Final Report prepared for Canadair, May, 1994.

8 Mingione, G., Brandi, V. and Esposito, B., "Ice Accretion Prediction on Multi-Element Airfoils," AIAA 97-0177, Jan. 1997.

9 Wright, W. B., and Rutkowski, A., "Validation Results for LEWICE 2.0," NASA CR 208690, Feb. 1999.

10 Ruff, G. A. and Anderson, D. N., "Quantification of Ice Accretions for Icing Scaling Evaluations," AIAA 98-0195, Jan. 1998.

11 Wright, W. B. and Potapczuk, M. G., "Comparison of LEWICE 1.6 and LEWICE/NS with IRT Experimental Data from Modern Airfoil Tests," AIAA 97-0175, Jan. 1997.

12 Wright, W.B., "Capabilities of LEWICE 1.6 and Comparison with Experimental Data," presented at the SAE/AHS International Icing Symposium, Sept. 1995.

13 Olsen, W., Shaw, R., and Newton, J., "Ice Shapes and the Resulting Drag Increase for a NACA 0012 Airfoil," NASA TM-83556, Jan. 1983.

14 Gray, V. H., "Correlations Among Ice Measurements, Impingement Rates, Icing Conditions, and Drag Coefficients for Unswept NACA 65A004 Airfoil," NACA TN4151, Feb. 1958.

15 Papadakis, M., Alansatan, S., and Seltmann, M., "Experimental Study of Simulated Ice Shapes on a NACA0011 Airfoil," AIAA 99-0096, Jan. 1999.

16 Kim, H. S., and Bragg, M. B., "Effects of Leading Edge Ice Accretion Geometry on Airfoil Aerodynamics," AIAA 99-3150, June 1999.

17 Addy, G.E., Potapczuk, M. G., and Sheldon, D., "Modern Airfoil Ice Accretions," AIAA -97-0174, Jan. 1997.

18 Spalart, P. R., and Allmaras, S. R., "A One-Equation Turbulence Model for Aerodynamic Flows," AIAA 92-0439, 1992.

19 Chung, J., Choo, Y., Reehorst, A., Potapczuk, M. and Slater, J., "Naviér-Stokes Analysis of the Flowfield Characteristics of an Ice Contaminated Aircraft Wing," AIAA 99-0375, Jan. 1999.

20 Chawner, J. and Steinbrenner, J., "Automatic Grid Generation Using GRIDGEN," NASA CP-3291, Surface Modeling, Grid Generation, and Related Issues in CFD Solutions, May 1995.

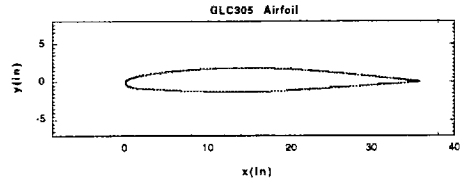

FIGURE 1. GLC305 Airfoil

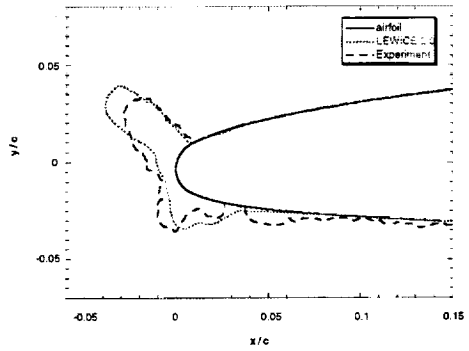

FIGURE 2. Run 937 Comparison

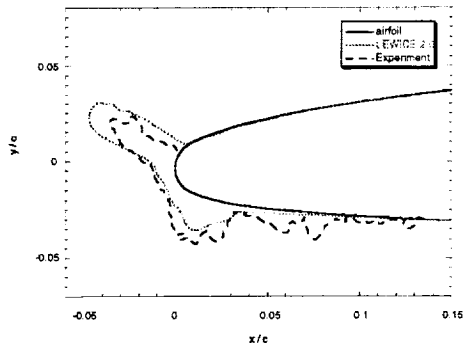

FIGURE 3. Run 204 Comparison

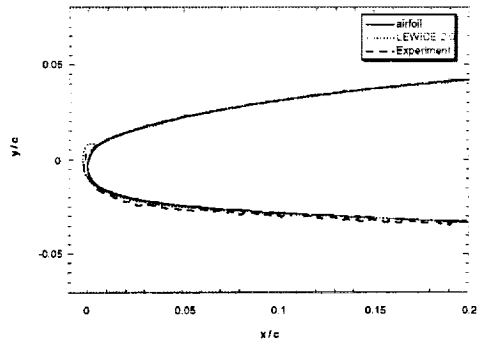

FIGURE 4. Run 202 Comparison

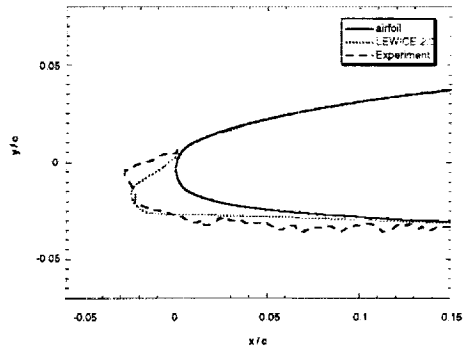

FIGURE 7. Run 212 Comparison

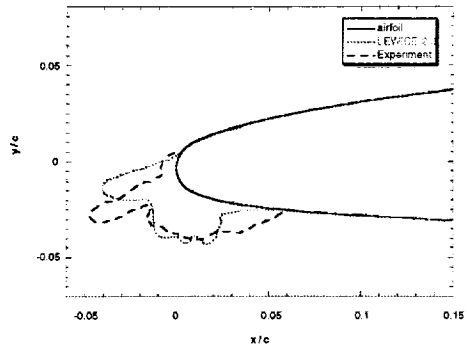

FIGURE 5. Run 912 Comparison

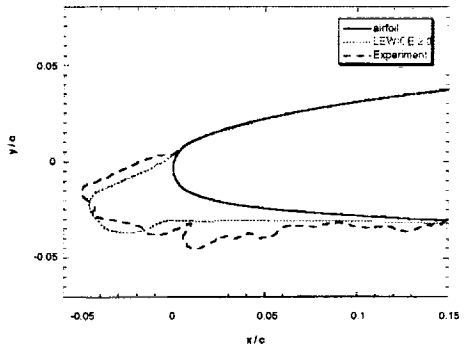

FIGURE 8. Run 916 Comparison

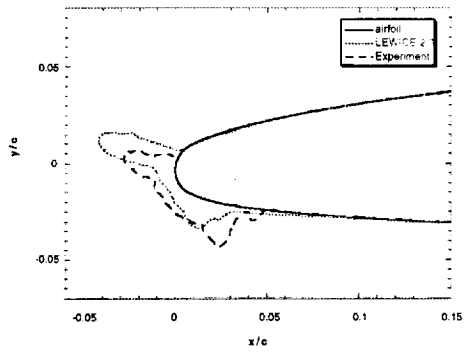

FIGURE 6. Run 907 Comparison

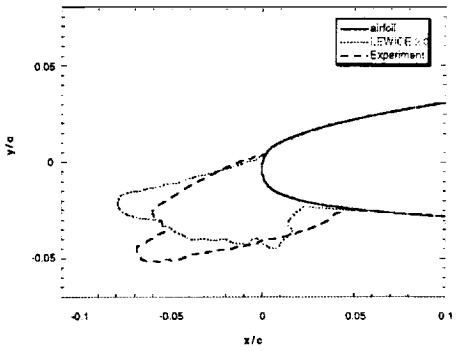

FIGURE 9. Run 913 Comparison

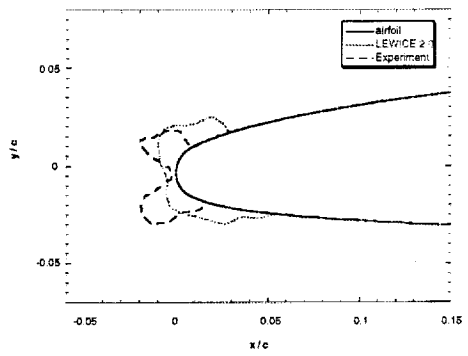

FIGURE 10. Run 941 Comparison

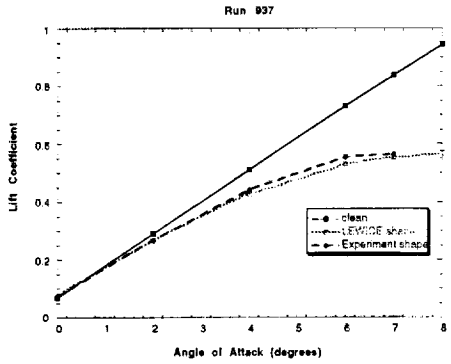

FIGURE 12. Run 937 Lift Comparison

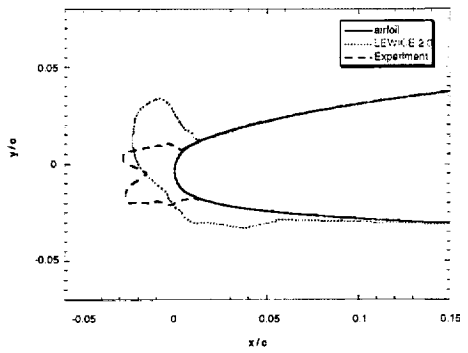

FIGURE 11. Run 943 Comparison

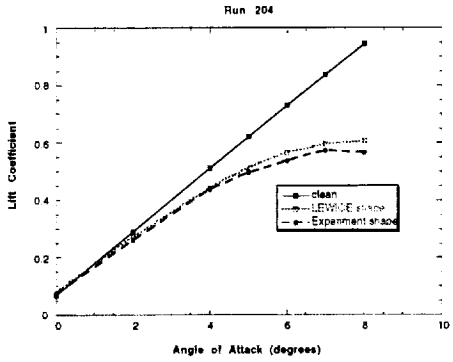

FIGURE 13. Run 204 Lift Comparison

Run #	Mach #	P_S	T_S	$Re*10^6$
		psi	R	
202	0.28	16	535	6.23
204	0.28	16	535	6.23
907	0.28	16	535	6.23
912	0.28	16	535	6.23
916	0.28	16	535	6.23
941	0.28	16	535	6.23
943	0.28	16	535	6.23
212	0.28	13.5	464	6.32
913	0.28	12.6	474	5.79
937	0.28	12.6	474	5.79

TABLE 1. Input Flow Conditions for WIND Cases

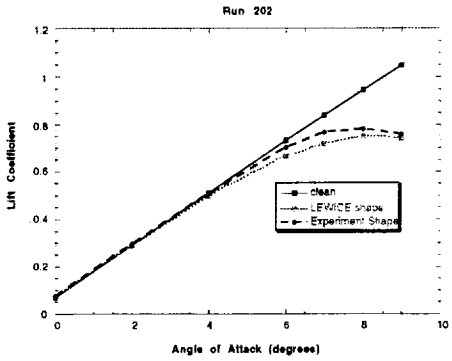

FIGURE 14. Run 202 Lift Comparison

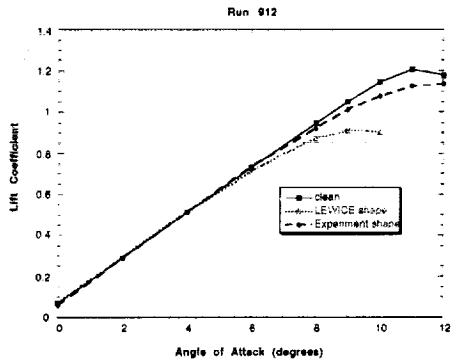

FIGURE 15. Run 912 Lift Comparison

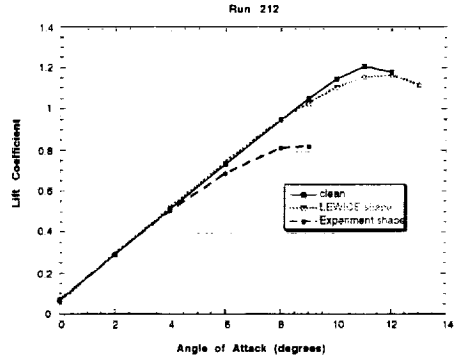

FIGURE 18. Run 212 Lift Comparison

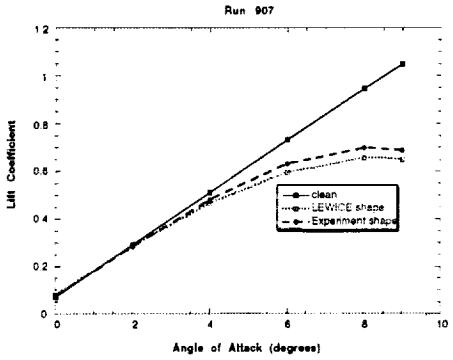

FIGURE 16. Run907 Lift Comparison

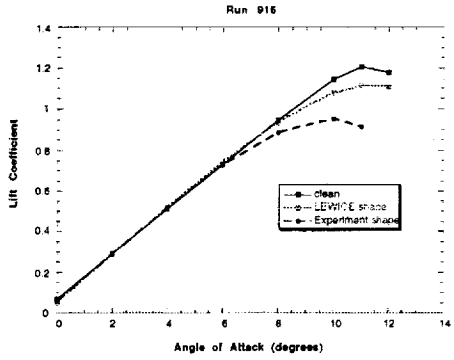

FIGURE 19. Run 916 Lift Comparison

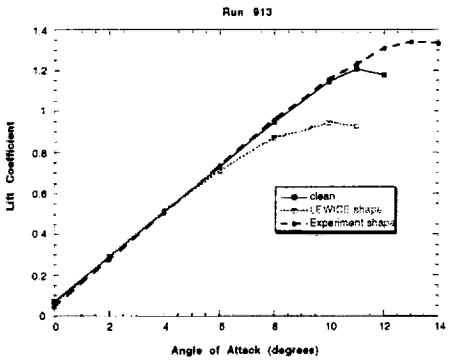

FIGURE 17. Run 913 Lift Comparison

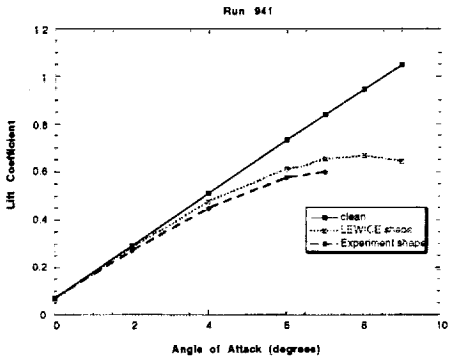

FIGURE 20. Run 941 Lift Comparison

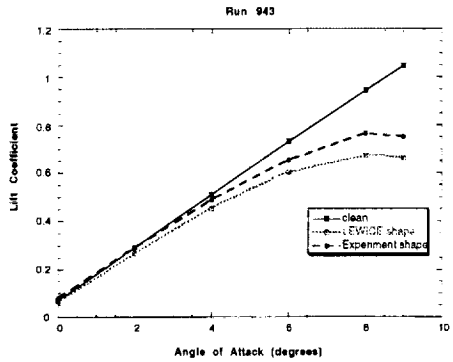

FIGURE 21. Run 943 Lift Comparison

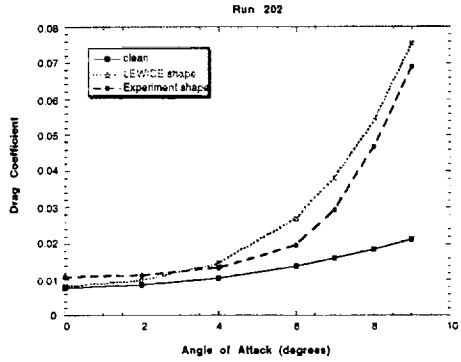

FIGURE 24. Run 202 Drag Comparison

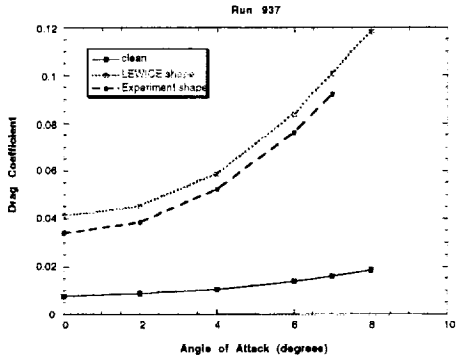

FIGURE 22. Run 937 Drag Comparison

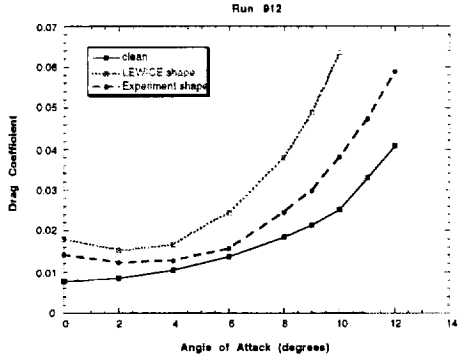

FIGURE 25. Run 912 Drag Comparison

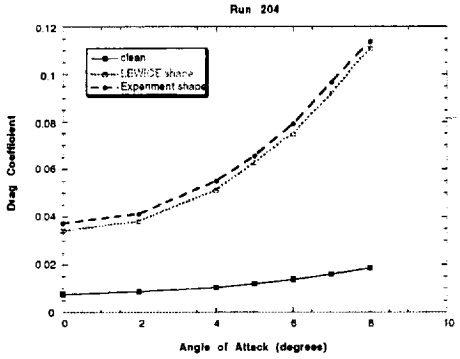

FIGURE 23. Run 204 Drag Comparison

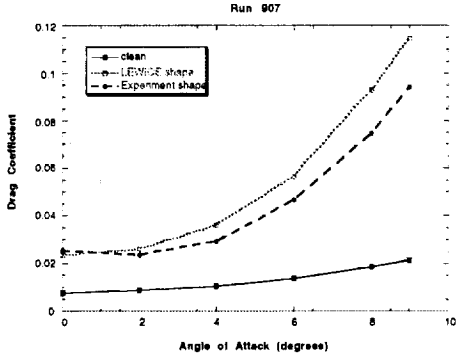

FIGURE 26. Run 907 Drag Comparison

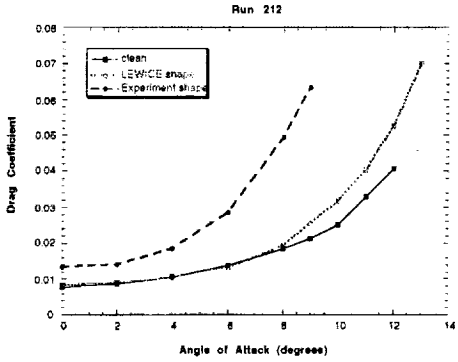

FIGURE 27. Run 212 Drag Comparison

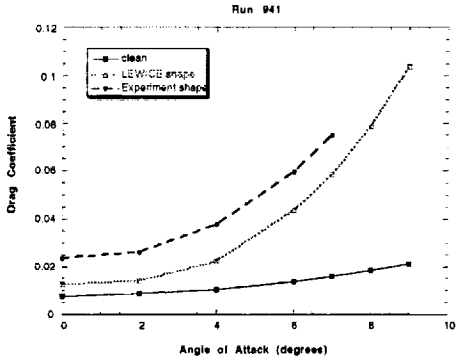

FIGURE 30. Run 941 Drag Comparison

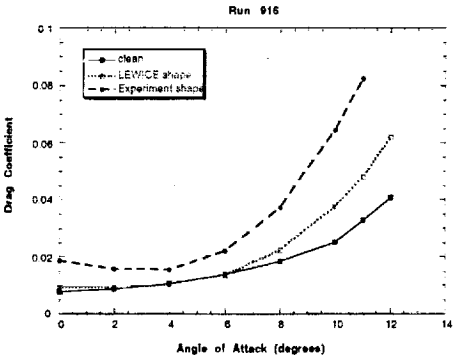

FIGURE 28. Run 916 Drag Comparison

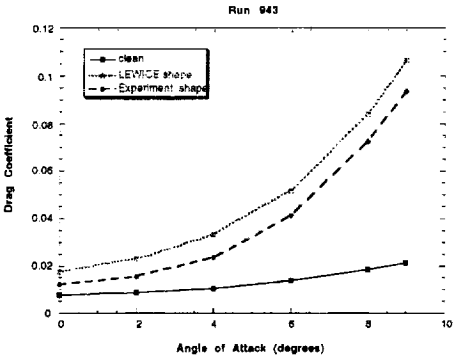

FIGURE 31. Run 943 Drag Comparison

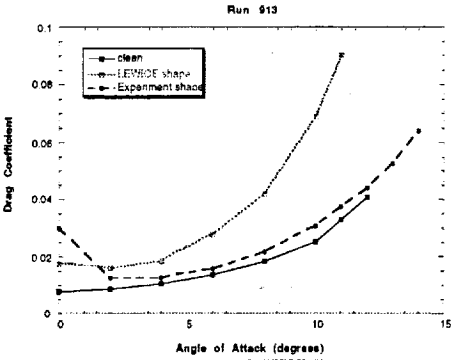

FIGURE 29. Run 913 Drag Comparison

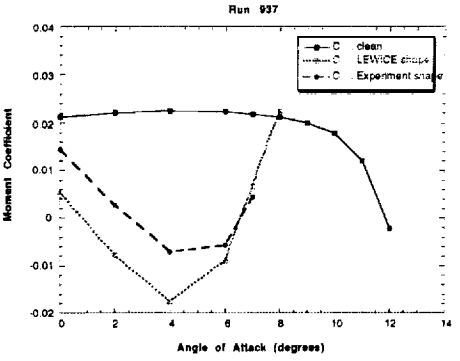

FIGURE 32. Run 937 Pitching Moment Comparison

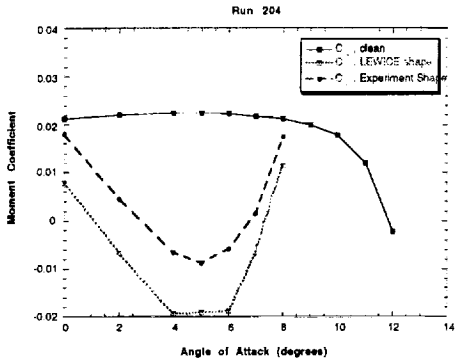

FIGURE 33. Run 204 Pitching Moment Comparison

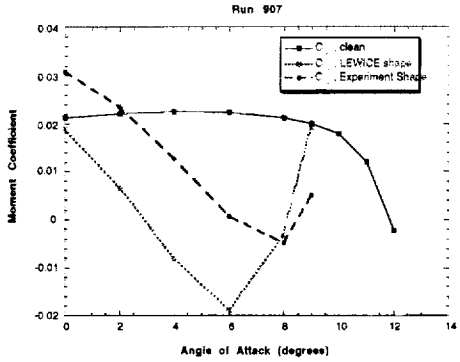

FIGURE 36. Run 907 Pitching Moment Comparison

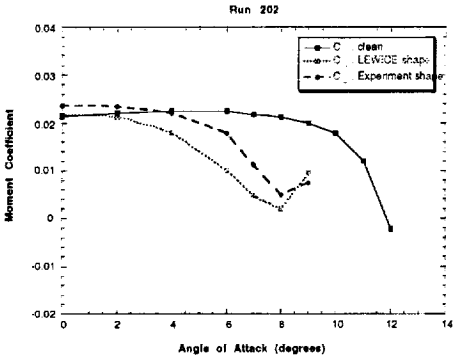

FIGURE 34. Run 202 Pitching Moment Comparison

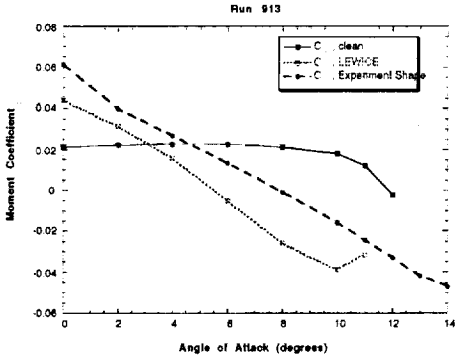

FIGURE 37. Run 913 Pitching Moment Comparison

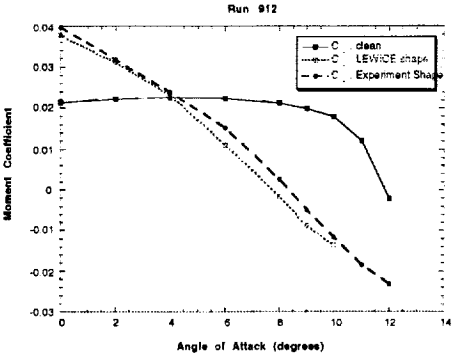

FIGURE 35. Run 912 Pitching Moment Comparison

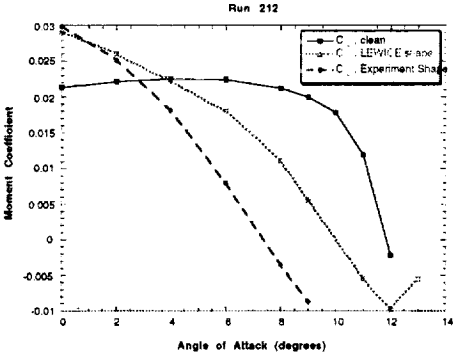

FIGURE 38. Run 212 Pitching Moment Comparison

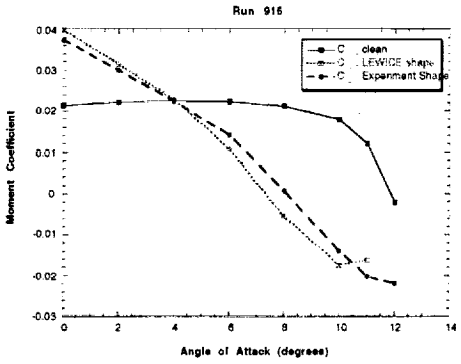

FIGURE 39. Run 916 Pitching Moment Comparison

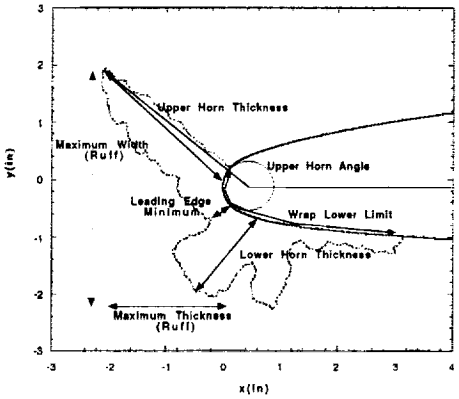

FIGURE 42. Ice Shape Geometric Measurements

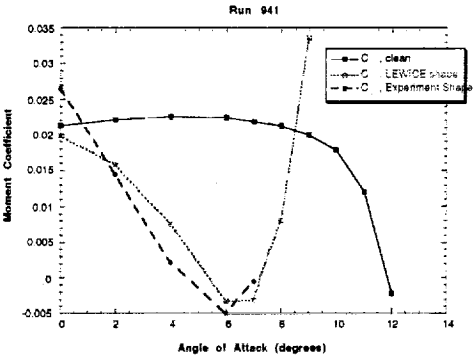

FIGURE 40. Run 941 Pitching Moment Comparison

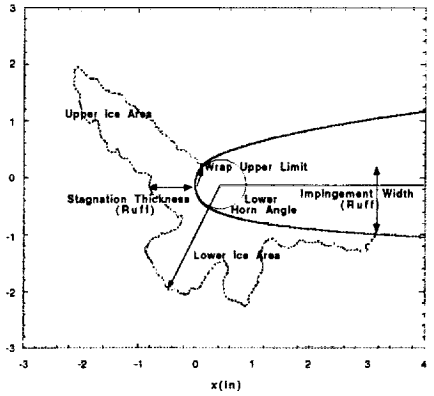

FIGURE 43. Additional Geometric Measurements

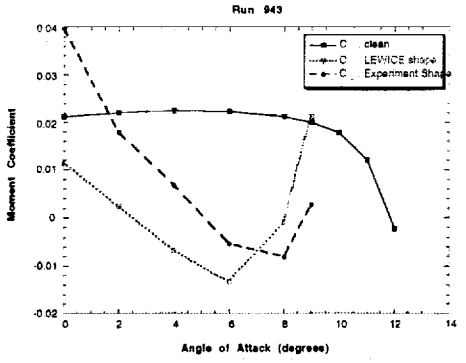

FIGURE 41. Run 943 Pitching Moment Comparison

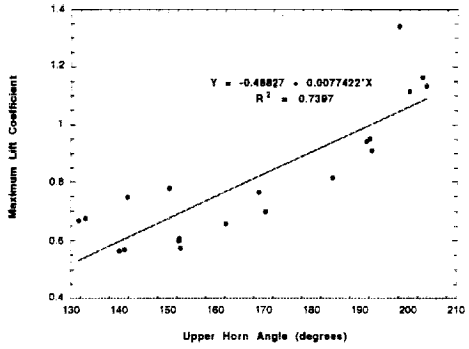

FIGURE 44. Maximum Lift Coefficient vs. Upper Horn Angle

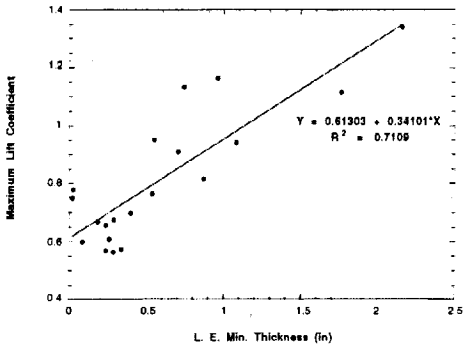

FIGURE 45. Maximum Lift Coefficient vs. Leading Edge Thickness

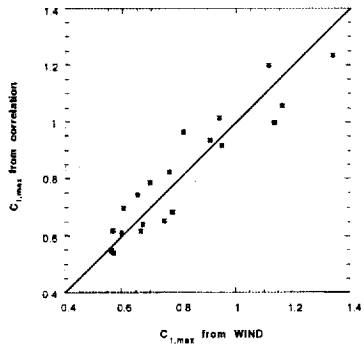

FIGURE 48. Calculated Lift Coefficients from Regression Equation (3)

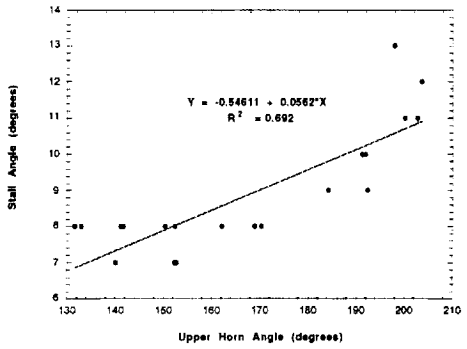

FIGURE 46. Stall Angle vs. Upper Horn Angle

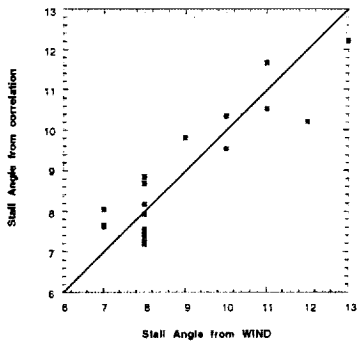

FIGURE 49. Calculated Stall Angle from Regression Equation (2)

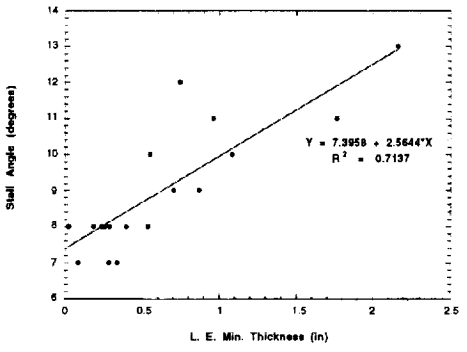

FIGURE 47. Stall Angle vs. Leading Edge Thickness

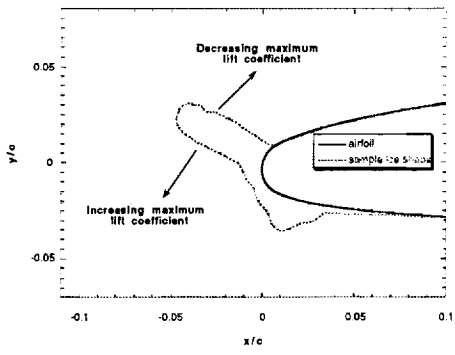

FIGURE 50. Effect of Horn Angle Change on Max. Lift

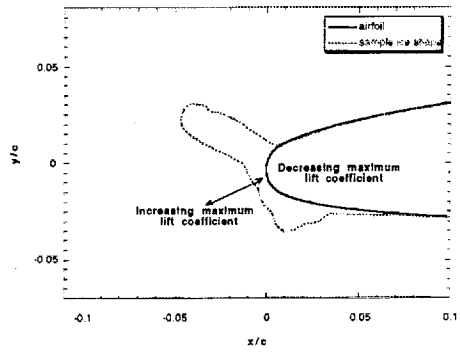

FIGURE 51. Effect of L.E. Thickness on Max. Lift

α	R^2 for Upper Horn Thickness	R^2 for Upper Horn Angle
0	0.195	0.099
2	0.023	0.256
4	0.0026	0.351
5	2*10-7	0.398
6	0.0009	0.459
7	0.0074	0.459
8	0.032	0.468

TABLE 2. R^2 values for Drag Regression Equations

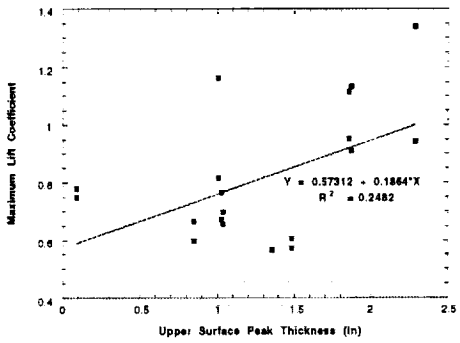

FIGURE 52. Lift Coefficient vs. Upper Horn Thickness

α	R^2 for Second Fourier Term
0	0.375
2	0.450
4	0.448
5	0.450
6	0.438
7	0.409
8	0.428

TABLE 3. R^2 values for Drag Regression Equations using Frequency-weighted average of Fourier Coefficients

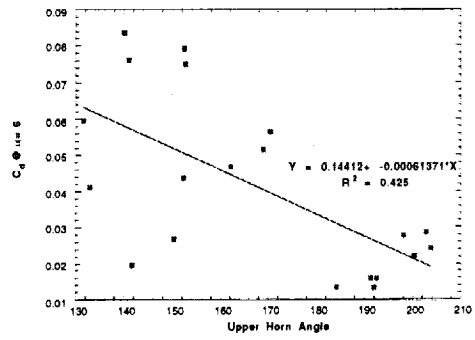

FIGURE 53. Drag Coefficient vs. Upper Horn Angle

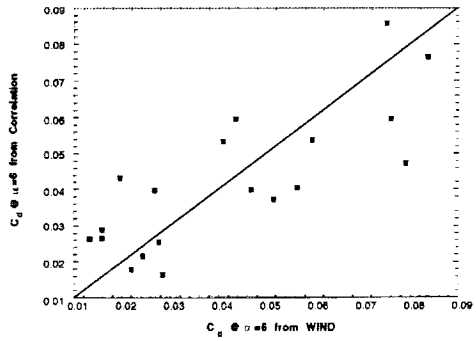

FIGURE 54. Calculated Drag from Regression Equation

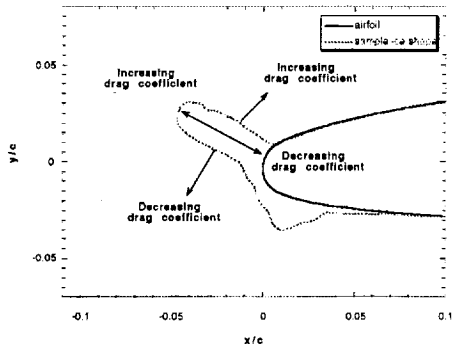

FIGURE 55. Effect of Horn Angle and Thickness on Drag

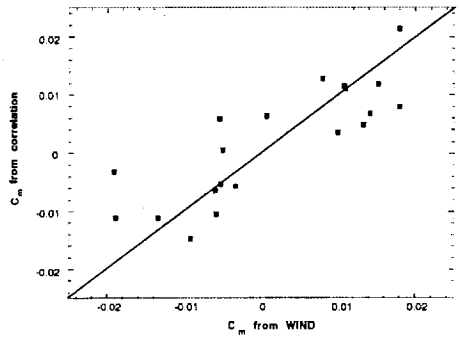

FIGURE 58. Calculated Pitching Moment from Regression Equation

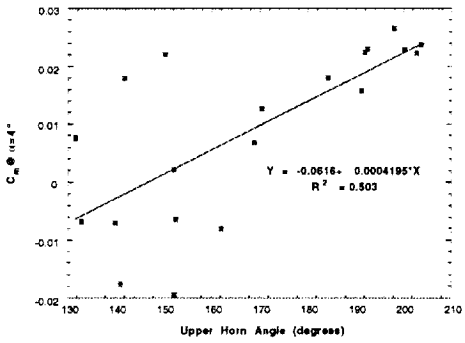

FIGURE 56. Pitching Moment vs. Upper Horn Angle

α	R^2 for Upper Horn Thickness	R^2 for Upper Horn Angle	R^2 for Lower Horn Thickness
0	-------	0.645	0.564
2	-------	0.611	-------
4	0.004	0.503	-------
5	0.015	0.461	-------
6	0.035	0.366	-------
7	0.045	0.066	-------

TABLE 4. R^2 values for Pitching Moment Regression Equations

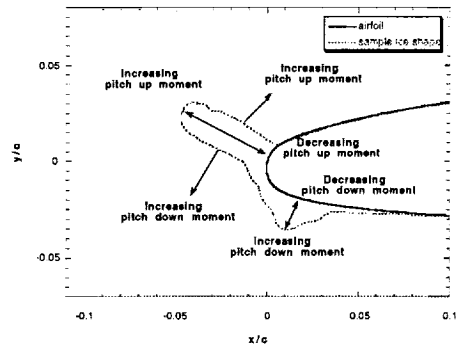

FIGURE 57. Effect of Horn Angle and Thicknesses on Pitching Moment

Measurement	$R^2_{measurement}$	R^2_{effect}	w_f
Lift Terms			
L.E. Min. Thickness	0.7125	0.8095	0.1807
Upper Horn Angle	0.7085	0.8095	0.1797
Average Fourier Coefficient	0.1225	0.8095	0.0311
Drag Terms			
Upper Horn Thickness	0.0373	0.6209	0.0136
Upper Horn Angle	0.3557	0.6209	0.1301
Average Fourier Coefficient	0.4283	0.6209	0.1566
Pitching Moment Terms			
Lower Horn Thickness	0.094	0.6373	0.0524
Upper Horn Thickness	0.0165	0.6373	0.0092
Upper Horn Angle	0.442	0.6373	0.2466
Overall Factors			
Upper Horn Angle			0.5564
Average Fourier Coefficient			0.1877
L.E. Min. Thickness			0.1807
Lower Horn Thickness			0.0524
Upper Horn Thickness			0.0228

TABLE 5. Weighting Factors for Geometric Terms

Run#	OCF	Δ Cl, max	Δ Stall Angle	ΔCd (Avg.)	ΔCm (Avg.)
202	0.108	0.03	0	0.0102	0.0143
204	0.079	0.035	1	0.0105	0.0027
212	0.196	0.348	2	0.0198	0.0170
907	0.122	0.042	0	0.0147	0.0032
912	0.119	0.224	3	0.0073	0.0071
913	0.117	0.397	3	0.0144	0.0036
916	0.172	0.163	1	0.0098	0.0128
937	0.046	0.004	1	0.0049	0.0042
941	0.248	0.068	1	0.0036	0.0103
943	0.381	0.091	0	0.0169	0.0081

TABLE 6. Differences in Aerodynamic Parameters and the Overall Comparison Factor

REPORT DOCUMENTATION PAGE

Form Approved
OMB No. 0704-0188

1. AGENCY USE ONLY (*Leave blank*)	2. REPORT DATE	3. REPORT TYPE AND DATES COVERED
	December 1999	Final Contractor Report

4. TITLE AND SUBTITLE

Correlation Between Geometric Similarity of Ice Shapes and the Resulting Aerodynamic Performance Degradation—A Preliminary Investigation Using WIND

5. FUNDING NUMBERS

WU–548–20–23–00
NAS3–98008

6. AUTHOR(S)

William B. Wright and James Chung

7. PERFORMING ORGANIZATION NAME(S) AND ADDRESS(ES)

Dynacs Engineering Company, Inc.
2001 Aerospace Parkway
Brook Park, Ohio 44142

8. PERFORMING ORGANIZATION REPORT NUMBER

E–12057

9. SPONSORING/MONITORING AGENCY NAME(S) AND ADDRESS(ES)

National Aeronautics and Space Administration
John H. Glenn Research Center at Lewis Field
Cleveland, Ohio 44135–3191

10. SPONSORING/MONITORING AGENCY REPORT NUMBER

NASA CR—1999-209417
AIAA–2000–0097

11. SUPPLEMENTARY NOTES

Prepared for the 38th Aerospace Sciences Meeting and Exhibit sponsored by the American Institute of Aeronautics and Astronautics, Reno, Nevada, January 10–13, 2000. William B. Wright, Dynacs Engineering Company, Inc., Brook Park, Ohio 44142, and James Chung, Institute for Computational Mechanics in Propulsion, Cleveland, Ohio 44142. Project Manager, Mary Wadel, Turbomachinery and Propulsion Systems Division, NASA Glenn Research Center, organization code 5830, (216) 977–7510.

12a. DISTRIBUTION/AVAILABILITY STATEMENT

Unclassified - Unlimited
Subject Categories: 02 and 08 Distribution: Nonstandard

This publication is available from the NASA Center for AeroSpace Information, (301) 621–0390.

12b. DISTRIBUTION CODE

13. ABSTRACT ***(Maximum 200 words)***

Aerodynamic performance calculations were performed using WIND on ten experimental ice shapes and the corresponding ten ice shapes predicted by LEWICE 2.0. The resulting data for lift coefficient and drag coefficient are presented. The difference in aerodynamic results between the experimental ice shapes and the LEWICE ice shapes were compared to the quantitative difference in ice shape geometry presented in an earlier report. Correlations were generated to determine the geometric features which have the most effect on performance degradation. Results show that maximum lift and stall angle can be correlated to the upper horn angle and the leading edge minimum thickness. Drag coefficient can be correlated to the upper horn angle and the frequency-weighted average of the Fourier coefficients. Pitching moment correlated with the upper horn angle and to a much lesser extent to the upper and lower horn thicknesses

14. SUBJECT TERMS

Icing

15. NUMBER OF PAGES

28

16. PRICE CODE

A03

17. SECURITY CLASSIFICATION OF REPORT	18. SECURITY CLASSIFICATION OF THIS PAGE	19. SECURITY CLASSIFICATION OF ABSTRACT	20. LIMITATION OF ABSTRACT
Unclassified	Unclassified	Unclassified	